ADVANCED MATERIALS
www.advmat.de

A Zwitterionic Polyurethane Nanoporous Device with Low Foreign-Body Response for Islet Encapsulation

*Qingsheng Liu, Xi Wang, Alan Chiu, Wanjun Liu, Stephanie Fuchs, Bo Wang, Long-Hai Wang, James Flanders, Yidan Zhang, Kai Wang, Juan M. Melero-Martin, and Minglin Ma**

Encapsulation of insulin-producing cells is a promising strategy for treatment of type 1 diabetes. However, engineering an encapsulation device that is both safe (i.e., no cell escape and no breakage) and functional (i.e., low foreign-body response (FBR) and high mass transfer) remains a challenge. Here, a family of zwitterionic polyurethanes (ZPU) with sulfobetaine groups in the polymer backbone is developed, which are fabricated into encapsulation devices with tunable nanoporous structures via electrospinning. The ZPU encapsulation device is hydrophilic and fouling-resistant, exhibits robust mechanical properties, and prevents cell escape while still allowing efficient mass transfer. The ZPU device also induces a much lower FBR or cellular overgrowth upon intraperitoneal implantation in C57BL/6 mice for up to 6 months compared to devices made of similar polyurethane without the zwitterionic modification. The therapeutic potential of the ZPU device is shown for islet encapsulation and diabetes correction in mice for ≈3 months is demonstrated. As a proof of concept, the scalability and retrievability of the ZPU device in pigs and dogs are further demonstrated. Collectively, these attributes make ZPU devices attractive candidates for cell encapsulation therapies.

1. Introduction

Type 1 diabetes (T1D), an autoimmune disease in which insulin-producing pancreatic β-cells are mistakenly destroyed by the body's immune system, affects millions of people worldwide.[1] Although islet transplantation has shown promise in improving glycemic control in some T1D patients,[2] its broad application for larger T1D population has been limited by the shortage of donor islets and the need for long-term immuno-suppression. The development of human embryonic stem cell (hESC)-derived insulin-producing cells have expanded the feasibility of cell-mediated therapies for T1D by providing an unlimited supply of β-cells for transplantation.[3] However, immunosuppression and long-term safety remain challenges. Hence, there is an urgent need for an immunoprotective encapsulation device that is both safe, by allowing no cell escape or device breakage, and functional, by supporting long-term cell function with low foreign-body response (FBR) and efficient mass transfer.

There are currently two major strategies of encapsulation under research and development: Microscopic and macroscopic encapsulations.[4] In microencapsulation, alginate microcapsules—one of the most studied islet encapsulation platforms—can provide ample mass transfer to maintain survival and function of islets.[5] However, full graft retrieval remains a critical limitation, posing safety concerns and risks for clinical applications. Macroscopic devices on the other hand, such as hydrogel fibers, thin sheets, and diffusion chambers, have been developed as an alternative strategy for islet encapsulation.[6] Although hydrogel-based macroscopic devices, such as, alginate and polyethylene glycol, are relatively biocompatible and have facile mass transfer,[2e,6a,7] their mechanical strength is typically low. Moreover, the intrinsic softness and open-network structure of hydrogels may inadvertently allow for cell entrance

Dr. Q. Liu, X. Wang, Dr. A. Chiu, Dr. W. Liu, S. Fuchs, Dr. B. Wang, Dr. L.-H. Wang, Prof. M. Ma
Department of Biological and Environmental Engineering
Cornell University
Ithaca, NY 14853, USA
E-mail: mm826@cornell.edu

Prof. J. Flanders
Department of Biomedical Sciences
Cornell University
Ithaca, NY 14853, USA

The ORCID identification number(s) for the author(s) of this article can be found under https://doi.org/10.1002/adma.202102852.

DOI: 10.1002/adma.202102852

Y. Zhang
Department of Fiber Science and Apparel Design
Cornell University
Ithaca, NY 14853, USA

Dr. K. Wang, Prof. J. M. Melero-Martin
Department of Cardiac Surgery
Boston Children's Hospital
Boston, MA 02115, USA

Dr. K. Wang, Prof. J. M. Melero-Martin
Department of Surgery
Harvard Medical School
Boston, MA 02115, USA

Prof. J. M. Melero-Martin
Harvard Stem Cell Institute
Cambridge, MA 02138, USA

and escape. In other efforts, macroscopic devices made of conventional polymers such as, poly(tetrafluoroethylene) or polycaprolactone were mechanically robust and were effective in preventing cell escape.[8] However, fibrotic overgrowth around these devices impeded mass transfer across device and made device retrieval difficult.

Recently, zwitterionic materials have attracted attention for cell encapsulation applications owing to their hydrophilic nature and biocompatibility.[9] Our group previously reported zwitterionically modified alginate and triazole-zwitterionic hydrogels that mitigated fibrotic deposition and were applied for therapeutic islet encapsulation applications.[10] However, the relatively low mechanical strength of hydrogel materials limits their long-term practical use and clinical potential. Polyurethanes, a class of mechanically robust materials ranging from soft elastomers to rigid plastics, have been widely used in many biomedical applications. Typical polyurethanes, however, are hydrophobic, a property unfavorable for diffusion in aqueous environment (i.e., glucose and insulin to and from the islets) or mitigation of fibrotic reactions.[11] We hypothesize that an encapsulation device made of zwitterionic polyurethane (ZPU) may be a suitable candidate for islet encapsulation. In ZPU, the polyurethane backbone ensures mechanical robustness, while the zwitterionic motif contributes to the improvement of hydrophilicity, mass transfer, antifouling property, and biocompatibility of the device.

To this end, we developed a family of ZPU polymers and used an electrospinning technique to fabricate nanoporous encapsulation devices that integrated several desirable attributes for islet transplantation. First, the ZPU device was robust with a fracture strain of >2.5 and tensile stress of >10 MPa. Second, the ZPU nanofibrous membrane as the device wall was hydrophilic, allowing facile mass transfer, as confirmed by insulin diffusion and in vitro glucose-stimulated insulin secretion tests. Moreover, cell entrance and escape was likewise prevented by tuning the electrospun fiber size. Third, the ZPU device induced minimal cellular deposition (as low as ≈10 μm in thickness) in the intraperitoneal space of C57BL/6 mice with different implantation time points up to 6 months; the thickness of cellular deposition on the ZPU device were threefold lower relative to that on a similar polyurethane (PU) device without the zwitterionic modification. We showed that the ZPU device encapsulating rat islets enabled diabetes correction in chemically induced diabetic C57BL/6 mice for up to 3 months when the device was retrieved. Finally, as a preclinical proof of concept, we demonstrated the scalability, safety, and procedural feasibility (i.e., handling, implantation, and retrieval) of the device in both pigs and dogs. Given the balanced safety and function, this encapsulation design represents a promising candidate for the development of cell encapsulation therapies for T1D and other cell-based therapies.

2. Results

2.1. Design, Fabrication, and Characterization of the Zwitterionic Polyurethane Device

In this work, ZPU polymers were synthesized from sulfobetaine-diol (SB-Diol), poly(tetramethylene ether) glycol (PTMG), hexamethylene diisocyanate (HDI), and 1,4-diaminobutane (Figure S1, Supporting Information). The zwitterionic SB-Diol as a hard segment was synthesized (Figure S2, Supporting Information) and introduced to improve the hydrophilicity, antifouling properties, and biocompatibility of the ZPU polymers. A non-biodegradable PTMG with a molecular weight of 2 kDa was introduced as an elastic, soft segment of the polyurethanes. HDI was selected as a chemical building block, while 1,4-diaminobutane was selected as a chain extender to tune the molecular weight of the ZPU polymers. A family of ZPU polymers with various SB contents were synthesized as illustrated in **Figure 1**a and confirmed by NMR (Figure S2, Supporting Information). The synthesized ZPU were termed as ZPU-*x*, where *x* represents the molar ratios of SB-Diol: PTMG. A similar polyurethane without any SB content was synthesized as control and denoted as PU. We used electrospinning to fabricate tubular ZPU encapsulation devices (Figure 1b) with different dimensions (Inner diameter: 1–5 mm; wall thickness: 100–200 μm). The end of ZPU device was sealed by a thermal sealer. Scanning electron microscopy (SEM) image showed that the electrospun ZPU device possessed a nanoporous structure with randomly oriented nonwoven fibers (Figure 1c). X-ray photoelectron spectroscopy (XPS) analysis was used to determine the elemental compositions and SB moiety of ZPU membrane. Two peaks centered at 230 eV (binding energy, S_{2S}) and 168 eV (binding energy, S_{2p}) were detected in ZPU-2 membrane but not in PU membrane (Figure S3, Supporting Information), which is indicative of the sulfur atom from the SB group. Furthermore, PU and ZPU-2 membranes were distinguished from the N_{1S} spectrum (Figure 1d). The N_{1s} spectrum for the ZPU-2 consisted of two peaks, 402 eV from sulfobetaine's quaternary amine and 399 eV from urethane nitrogen, while only one peak (399 eV) was detected for PU. FT-IR results (Figure 1e) also showed a characteristic peak at 1037 cm^{-1} for ZPU-2 membrane, attributed to SO_3^-, confirming the existence of SB group. Moreover, the ZPU-2 membrane presented excellent thermal stability (Figure S3, Supporting Information)

Robust mechanical properties of device, critical for its handling, implantation and retrieval, are particularly desirable for cell encapsulation. Thus, the mechanical properties of ZPU membranes with various SB contents were investigated through tensile tests. Tensile strength and fracture strain of ZPU membranes (Figure 1f and Table S1, Supporting Information) decreased with increasing SB content. ZPU-1 membranes with low SB content were elastic, while ZPU-4 membranes with high SB contents became brittle. ZPU-2 membranes with medium SB content were shown to be mechanically robust (fracture strain of >2.5 and tensile stress of >10 MPa) (Figure 1f,g). In addition, ZPU-4 membranes became much weaker in wet condition as compared to those in dry condition, whereas ZPU-1 and ZPU-2 membranes exhibited similar mechanical strength in the two conditions. Histological studies (Figure 1h) revealed that the nanofibers of ZPU-4 device became loose while ZPU-2 device remained compact 1 month after intraperitoneal implantation in C57BL/6J mice. It was clear that the ZPU-4 device with high SB content was not suitable for cell encapsulation. We therefore chose ZPU-2 device with medium SB content, due to its balanced mechanical robustness and stability under in vivo

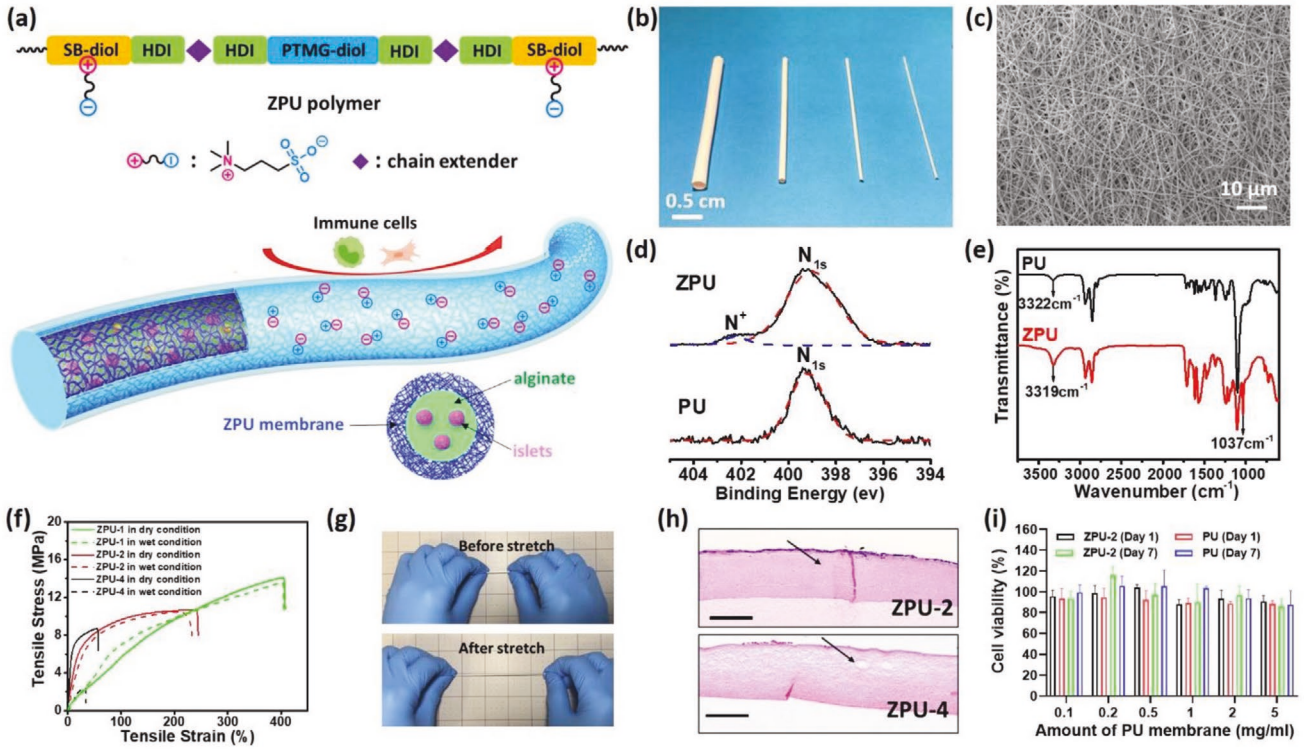

Figure 1. Design, fabrication, and characterization of the ZPU device. a) Schematic illustration of the chemical structure of the ZPU polymer and islet-containing ZPU device that mitigates FBR, prevents cell entrance or escape, and allows facile mass transfer. b) Digital images of ZPU devices with different sizes. c) A SEM image of the nanofibrous ZPU device. d) XPS N_{1s} spectra of the ZPU and PU membranes. e) FTIR spectra of the ZPU and PU membranes. f) Tensile test (stress–strain curves) of the ZPU membranes under dry or wet conditions. g) Stretching of a ZPU-2 device. h) H&E stained cross-sectional images of ZPU-2 and ZPU-4 devices, 30 day post intraperitoneal implantation in C57BL/6J mice. The arrows point to the integrity difference of the fiber structures after implantation. Scale bars: 200 μm. i) Cytotoxicity of ZPU-2 and PU membranes against NIH/3T3 fibroblasts determined by the MTT assay. Data are normalized to the negative control (i.e., cells cultured in the medium only) and expressed as mean ± standard error of the mean (S.E.M.) ($n = 6$).

conditions, for cell encapsulation in the following studies. MTT assays (Figure 1i) revealed negligible cytotoxicity of the ZPU-2 membrane.

2.2. The Safety of the Zwitterionic Polyurethane Device

The safety of an encapsulation device is of paramount importance for clinical applications especially when hESC-derived insulin-producing cells are used. A device needs to create a durable physical barrier to exclude the entrance of immune cells and also to prevent the encapsulated cells from escaping the device. In this work, we tuned the pore size for ZPU device by adjusting the fiber size to prevent cell entrance and escape (**Figure 2**a). As shown in Figure 2b,c, the fiber diameter and pore size were correlated and both increased with the concentration of the ZPU-2 polymer solution used in electrospinning (Figure S4, Supporting Information). To optimize the fiber diameter ensuring the safety, three kinds of ZPU-2 devices made from different polymer concentrations (10%, 15%, and 20% (g mL^{-1})), namely ZPU-10% with average fiber size of 281 nm and pore size of 386 nm, ZPU-15% with average fiber size of 483 nm and pore size of 805 nm, and ZPU-20% with average fiber size of 649 nm and pore size of 1197 nm, were fabricated by adjusting the polymer concentration.

To assess cell escape, GFP expressing cells (NIH3T3/GFP)-loaded gelatin/fibrinogen hydrogels were injected into the encapsulation device and cultured in cell culture media. The biodegradable gelatin/fibrinogen hydrogel matrix allowed for NIH3T3/GFP cells to proliferate and migrate. After a 5-day incubation period, some cells started to escape from the ZPU-15% and ZPU-20% devices (Figure S5, Supporting Information). A large number of cells further escaped from the two devices after day 12, while ZPU-10% devices with an average fiber diameter of 281 nm completely prevented cell escape all the times despite massive cell growth inside (Figure 2d). To assess the cell entrance, these three ZPU devices were implanted into the intraperitoneal space of C57BL/6J mice for 1 month. Histological staining showed that the ZPU-10% device completely excluded cell entrance and nearly all the cells were blocked by the outermost layer (Figure 2e). For the other two devices (ZPU-15% and ZPU-20%), different number of cells penetrated into the device and some even migrated into the interior for the ZPU-20% device with largest fiber size (Figure 2f). Therefore, the ZPU-10% device that was able to prevent cell entrance and escape, was selected as a cell encapsulation device in our following work.

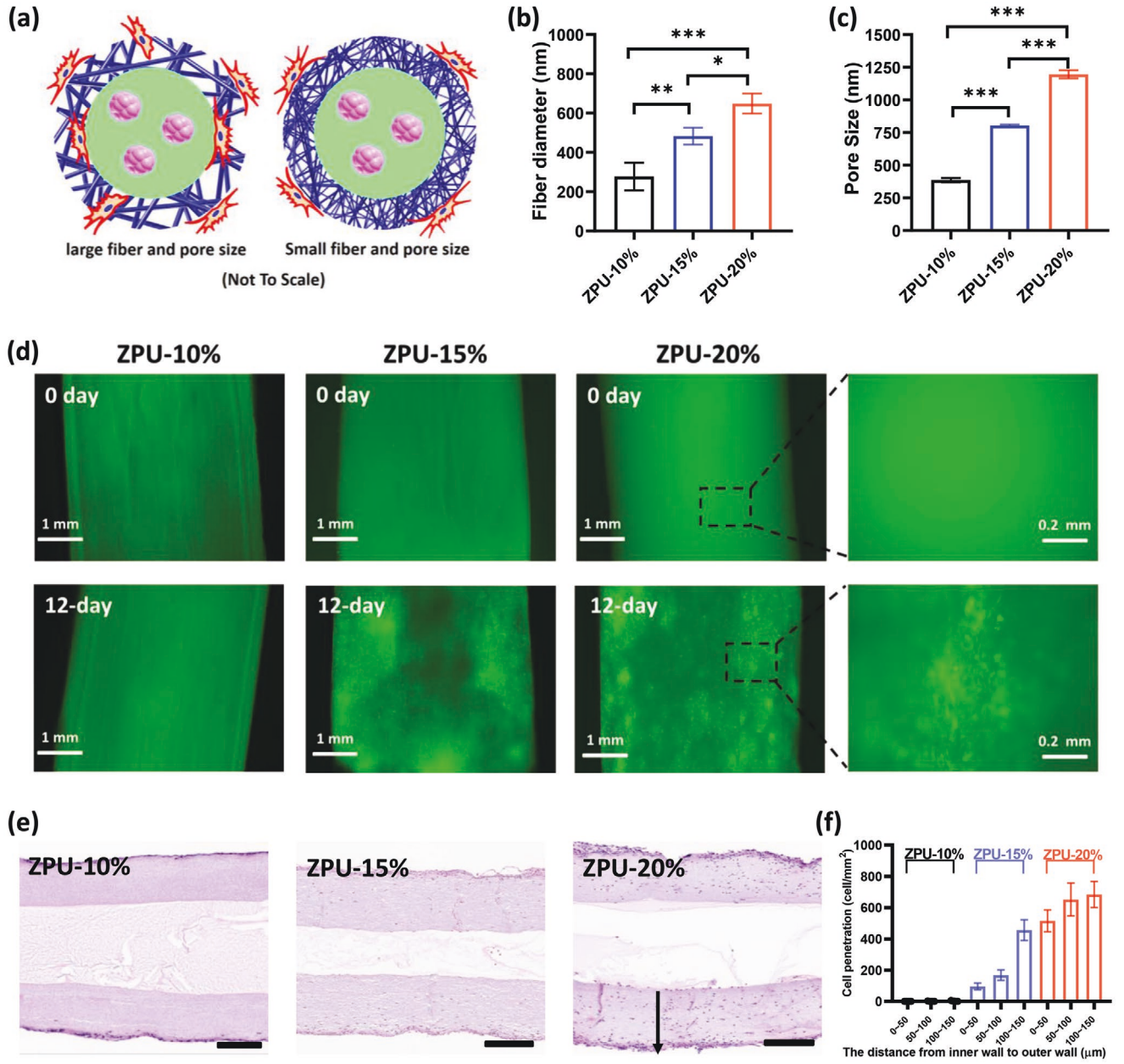

Figure 2. ZPU devices prevent cell entrance or escape. a) Schematic showing the prevention of cell entrance (or similarly cell escape) by adjusting the fiber and pore size. b) Fiber sizes of ZPU devices as a function of concentration of ZPU-2 polymer. $n = 4$ per group. *$p < 0.05$; **$p < 0.01$. c) Pore sizes of ZPU devices as a function of concentration of ZPU-2 polymer. $n = 3$ per group. ***$p < 0.001$. d) In vitro cell escape test of various ZPU devices made from different polymer concentrations (from left to right: 10%, 15%, and 20% ZPU-2). e) H&E staining images of retrieved ZPU devices, 1 month post intraperitoneal implantation in C57BL/6J mice ($n = 3$–4). Scale bar: 100 μm. The arrow points from the inner wall of the device to the outer wall. f) Quantification of cell entrance for various ZPU devices.

2.3. Antifouling and Mass Transfer Properties of Zwitterionic Polyurethane Device

Undesirable biofouling from proteins, cells, or bacteria is of great concern for many biomedical devices.[12] Specially, protein adsorption on the surface of medical devices is considered the initial and critical step in the FBR.[13] Moreover, insulin adsorption on devices was reported to reduce actual insulin delivery, resulting in less controllable glycemic control.[14] In general, hydrophilic surfaces are desirable for reducing nonspecific protein adsorption.[15] Water droplets wetted the ZPU surface (**Figure 3**a) almost immediately (within 3 s) due to the hydrophilic SB group and the nanoporous structures. In contrast, water droplets remained on the PU control membrane after 120 s. This comparison indicated that the incorporated SB group rendered ZPU membrane surface superhydrophilic. FITC-labelled insulin and fibrinogen as the two model proteins were used in our work to assess the antifouling performance of

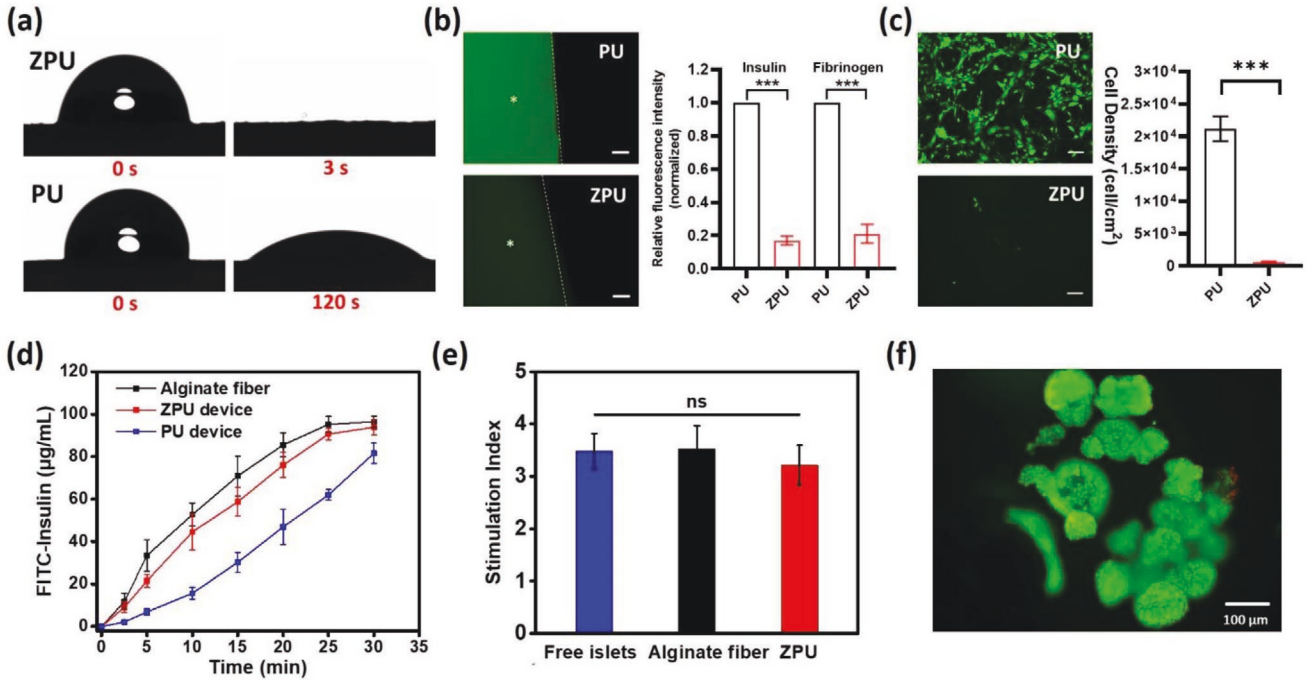

Figure 3. Hydrophilicity, antifouling and mass transfer characterizations of the ZPU device. a) Digital photographs of water droplets on ZPU and PU membranes. b) FITC-labeled insulin and fibrinogen adsorption on the ZPU and PU membranes. The asterisks indicate the location of the membrane and the dashed lines indicate the edge of membrane. Scale bars: 100 μm. Mean ± S.E.M. ($n = 3$); ***$p < 0.001$. c) NIH/3T3 cells attachment on ZPU and PU membranes after incubation for 3 days. Scale bars: 100 μm. Mean ± S.E.M. ($n = 5$); ***$p < 0.001$. d) Insulin diffusion from alginate fiber, PU, and ZPU devices as a function of time. $n = 3$ per group. e) In vitro GSIS of the encapsulated rat islets in ZPU device, compared to that of free islets and the islets encapsulated in alginate fibers. Mean ± S.E.M. ($n = 4$); ns, not significant. f) Live (green) and dead (red) staining of encapsulated islets in the ZPU device after 3-days culture.

the ZPU membrane, with the PU membrane used as control. Fibrinogen is a coagulation protein involved in platelet aggregation, blot clot formation, and fibrotic formation.[16] Relative to the PU membrane, the amount of insulin and fibrinogen adsorptions on ZPU membrane was 17.3% and 21.1%, respectively, thereby demonstrating that the ZPU surface was resistant to non-specific protein adsorption (Figure 3b and Figure S6, Supporting Information). We next investigated the cell attachment on the ZPU membrane in vitro. After incubation at 37 °C for 3 days, NIH/3T3 cells quickly attached, proliferated, and formed a confluent layer on the PU control membrane while there were only scattered cells observed on the ZPU membrane (Figure 3c). The cell densities on PU and ZPU surfaces were 2.1×10^4 and 4.3×10^2 cells cm^{-2}, respectively. These results indicate that ZPU membrane could reduce cell adhesion. In addition, bacterial contamination can cause failure of medical devices.[17] As shown in Figure S6, Supporting Information, very few bacteria were observed on the surface of ZPU membrane, compared to the PU control.

For an effective encapsulation device, transplanted cells must have an adequate nutrient and oxygen supply to maintain their function.[2a] We investigated whether the ZPU membrane as a physical barrier between the recipient and transplanted cells would allow sufficient mass transfer, as we would expect from its high porosity and superhydrophilic property. We designed and conducted an experiment to investigate the diffusion rate of insulin from the device. FITC-labeled insulin was mixed into alginate and loaded into ZPU device, with alginate hydrogel fibers and PU devices of similar dimension used as controls. Insulin diffusion out of the devices was monitored over time. As expected, alginate fibers without any physical barriers presented the fastest insulin diffusion, whereas ZPU devices showed lower but comparable diffusion rates (Figure 3d). In contrast, a much slower insulin diffusion was observed from the PU device. Next, a static glucose-stimulated insulin secretion (GSIS) experiment was conducted. Figure 3e and Figure S7, Supporting Information, showed that rat islets encapsulated in ZPU devices were responsive to glucose change and secreted insulin. The stimulation index (a ratio of the insulin amount following high glucose stimulation divided by that at low glucose condition) of islets in the ZPU device (3.21 ± 0.38) was similar to that of free islets (3.48 ± 0.34) and alginate fibers (3.53 ± 0.45). The live and dead staining (Figure 3f) showed high viability of islets inside the ZPU device after 3-day culture, further confirming that the ZPU device had sufficient mass transfer to support cell survival. Taken together, these results confirmed that the hydrophilic ZPU device allowed for efficient mass transfer.

2.4. In Vivo Biocompatibility of the Zwitterionic Polyurethane Device

The FBR and fibrotic cellular overgrowth are major challenges for cell encapsulation.[18] We evaluated the FBR against blank ZPU devices at different time points (2 weeks, 1 month,

3 months, and 6 months) after intraperitoneal implantation in C57BL/6J mice, a strain previously own to elicit a strong FBR against implants.[5a] The PU device was included as a control for comparison. At 14 days, the ZPU devices had a layer of cellular overgrowth around 7.2 ± 1.2 μm, while the PU devices induced a fibrotic deposition of 26.7 ± 3.8 μm (**Figure 4**a), suggesting that the zwitterionic SB moiety mitigated the cellular growth. Similar and consistent results were obtained in longer term studies (i.e., 1, 3, and 6 months) (Figure 4a): fibrotic layers on ZPU devices were significantly thinner as compared to those on PU control. The thickness on ZPU device at 1, 3, and 6 months was 6.0 ± 1.2, 7.7 ± 1.8, and 9.7 ± 2.2 μm, respectively, while the corresponding thickness on the PU device was 30.3 ± 4.3, 37.6 ± 6.5, and 38.9 ± 5.3 μm, respectively (Figure 4b). We also analyzed the composition and level of immune cells deposited on ZPU and PU devices through fluorescence-activated cell sorting (FACS). Compared to PU devices 1 month post implantation, ZPU devices had significantly less deposition of neutrophils, monocytes, macrophages, and dendritic cells that were involved in FBR (Figure 4c–f).[19] We also observed a much lower level of B and T cells deposited on ZPU device than PU device (Figure S8, Supporting Information). These quantifications suggest that ZPU devices substantially reduced cellular overgrowth in the intraperitoneal space of C57BL/6J mice in both short (14 days) and long (up to 180 days) time periods. Furthermore, all the ZPU devices (n = 21) implanted were easily retrieved without tissue adhesion, while 9 out of 22 PU devices had tissue adhesion (Figure S9, Supporting Information), making the retrieval difficult.

2.5. Testing of the Zwitterionic Polyurethane Device in Large Animals

We further tested the biocompatibility of ZPU device in large animals. We scaled up the ZPU device by using longer rotating templates during the electrospinning. The scaled-up ZPU device (≈1.8 mm in diameter and 10 inches in length) was inserted into a pipette, implanted intraperitoneally into Göttingen minipigs (n = 2), and placed near the liver using a minimally invasive laparoscopic procedure (Figure 4g,h). 5 weeks after implantation, the entire device except the end parts showed no tissue adhesion (Figure 4i). The tissue adhesion at the device ends, although considered minor, occurred in both pigs, likely because of the irritation caused by the stiff sealing edges. Nevertheless, the entire device was retrievable after excising the adhered tissue (Video S1, Supporting Information). H&E staining of retrieved devices revealed severe cellular deposition at the device ends (Figure 4j), but most of the central regions of the devices had thin cellular overgrowth (Figure 4k). We also implanted ZPU devices into the omentum of Beagle dogs (n = 2). The omentum is considered to be "the policeman of the abdomen" due to its strong reactions to foreign objects.[20] As expected, the device was completely embedded within the omentum after five weeks of implantation (Figure 4l). Interestingly, however, the adhered tissue from the majority of the device could be gently peeled off using laparoscopic forceps (Figure 4m and Video S2, Supporting Information). Similar to the outcome from the pig study, the cellular depositions on the middle parts of the devices were relatively thin (Figure 4n), despite much thicker fibrotic tissue at the device ends (Figure 4o). All of these results from the mouse, pig, and dog studies demonstrated the relative biocompatibility of the ZPU device.

2.6. Diabetes Correction in Mice

After confirming the mechanical, mass transfer, and antifouling properties, as well as, safety and biocompatibility of the ZPU device, we explored its therapeutic potential as a cell encapsulation platform for treatment of T1D. Rat islets mixed in an alginate solution were injected into the device and crosslinked by a mixture of calcium and barium ions. Alginate hydrogel in this work served as the extracellular matrix for encapsulated islets, due to its mild gelation conditions and negligible toxicity. The open end of the device was thermally sealed. Devices encapsulating rat islets (500-600 islet equivalents per mouse) were transplanted into the peritoneal cavity of streptozotocin (STZ)-induced diabetic C57BL/6J mice and evaluated for their ability to restore normoglycemia. **Figure 5**a shows the blood glucose concentrations (BG) over time post-transplantation. The BG of all mice dropped to normal glycemic range (BG < 200 mg dL^{-1}) within 1 week after transplantation. 8 out of the 13 mice remained normoglycemic for 2 months until the devices were retrieved. Some earlier failures occurred, likely due to unintentional variables such as the disintegration of cell-loaded alginate, device defects, and islet numbers, as well as, intrinsic biological variations. The BG of the cured mice went up after retrieval, confirming the device function. Furthermore, the devices were readily retrieved and there was no tissue adhesion. An intraperitoneal glucose tolerance test (IPGTT) (Figure 5b) was performed 2 months after transplantation. The engrafted mice gradually achieved normoglycemia within 90 min, while the BG of the diabetic mice remained high even after 120 min, further confirming the function of transplanted islets. GSIS test of the retrieved ZPU devices (Figure 5c) suggested that the islets were responsive to glucose change and secreted insulin, another evidence for islet function. In a separate 3-month transplantation experiment, 3 out of 4 mice were cured until retrieval. IPGTT and GSIS (Figure 5d,e) assays were conducted to verify the viability and function of transplanted islets. We also measured pancreatic insulin content of the engrafted, diabetic, and healthy mice (Figure 5f). The content of pancreatic insulin for the engrafted and diabetic mice was only 1% of that of healthy mice. This result indicated that the ZPU device was responsible for the blood glucose control.

Post-retrieval imaging and histological characterizations showed that there were numerous healthy rat islets in islet-loaded alginate hydrogel within the retrieved devices (Figure 5g). Many retrieved islets exhibited morphology as healthy as intact islets before transplantation, as shown by the H&E staining of cross-sections (Figure 5h). Although the FBR was slightly elevated by the encapsulated xenogeneic donor tissue, the cellular deposition around the ZPU devices was still relatively thin (≈8.9 ± 1.3 μm; Figure 5i and Figure S10, Supporting Information). The viability and function of retrieved islets were further verified by positive insulin staining

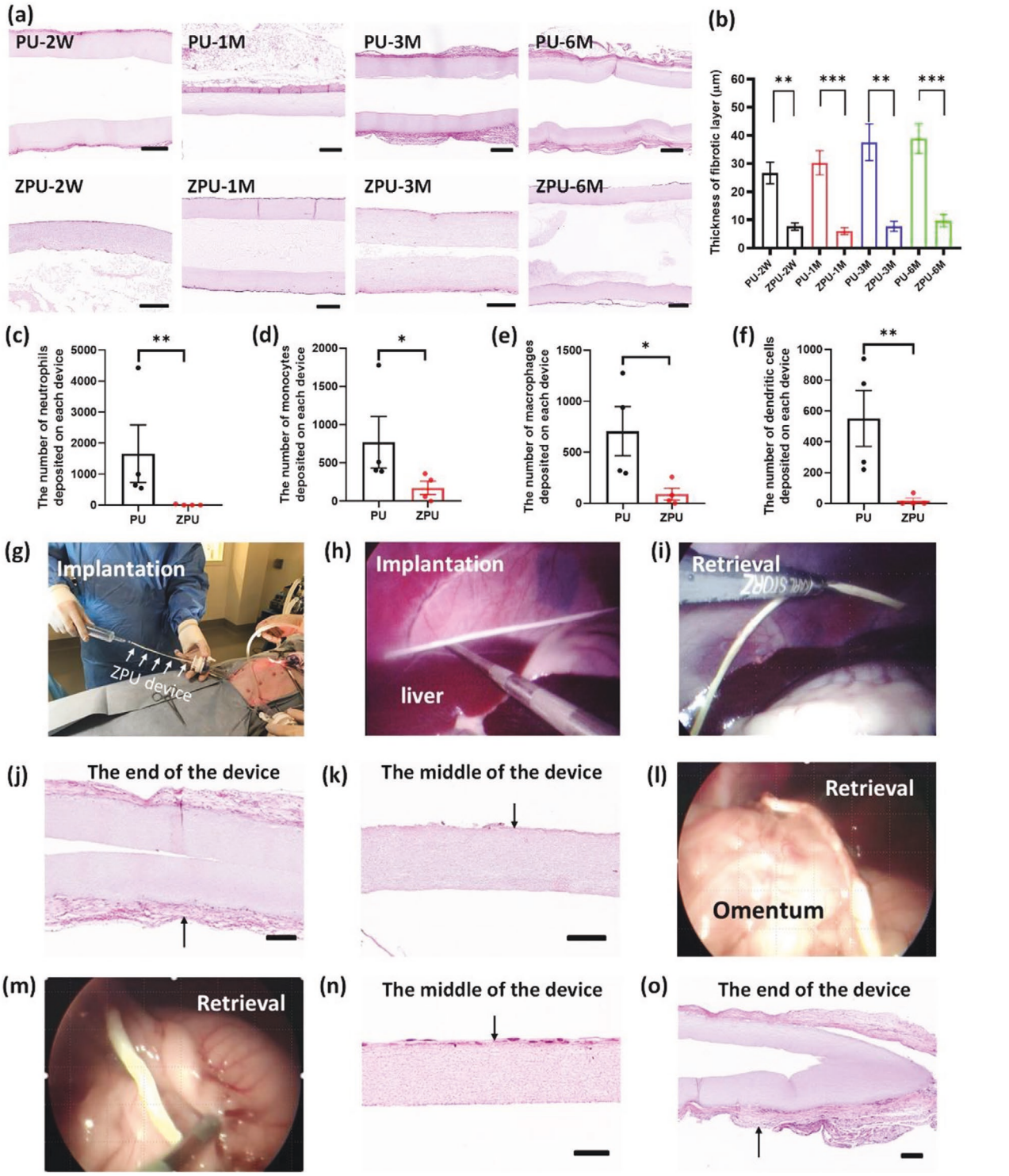

Figure 4. Biocompatibility tests of ZPU devices in mice, pigs, and dogs. a) Representative H&E staining images of blank PU and ZPU devices at different implantation time points. b) Analysis of the thickness of cellular overgrowth around devices measured from H&E staining images, mean ± S.E.M. (n = 3–5). $^{**}p < 0.01$; $^{***}p < 0.001$. c–f) The average levels of neutrophils, monocytes, macrophages, and dendritic cells deposited on each device, 1 month post intraperitoneal implantation in C57BL/6J mice. Mean ± S.E.M. (n = 4). $^{*}p < 0.05$; $^{**}p < 0.01$. g,h) A digital photo showing the implantation process in pigs (n = 2). i) Laparoscopic images showing the device being pulled out during retrieval, 35 days after intraperitoneal implantation in a pig. j) H&E stained cross-sectional image of the end of the device (scale bar: 100 μm). k) H&E stained cross-sectional image of the middle of the device (scale bar: 100 μm). l,m) Laparoscopic images during retrieval of ZPU devices, 35 days after intraperitoneal implantation in a dog (n = 2). n) H&E stained cross-sectional image of the middle of the device (scale bar: 100 μm). o) H&E stained cross-sectional image of the end of the device (scale bar: 100 μm). The arrows in (j), (k), (n), and (o) point to cellular depositions on the devices.

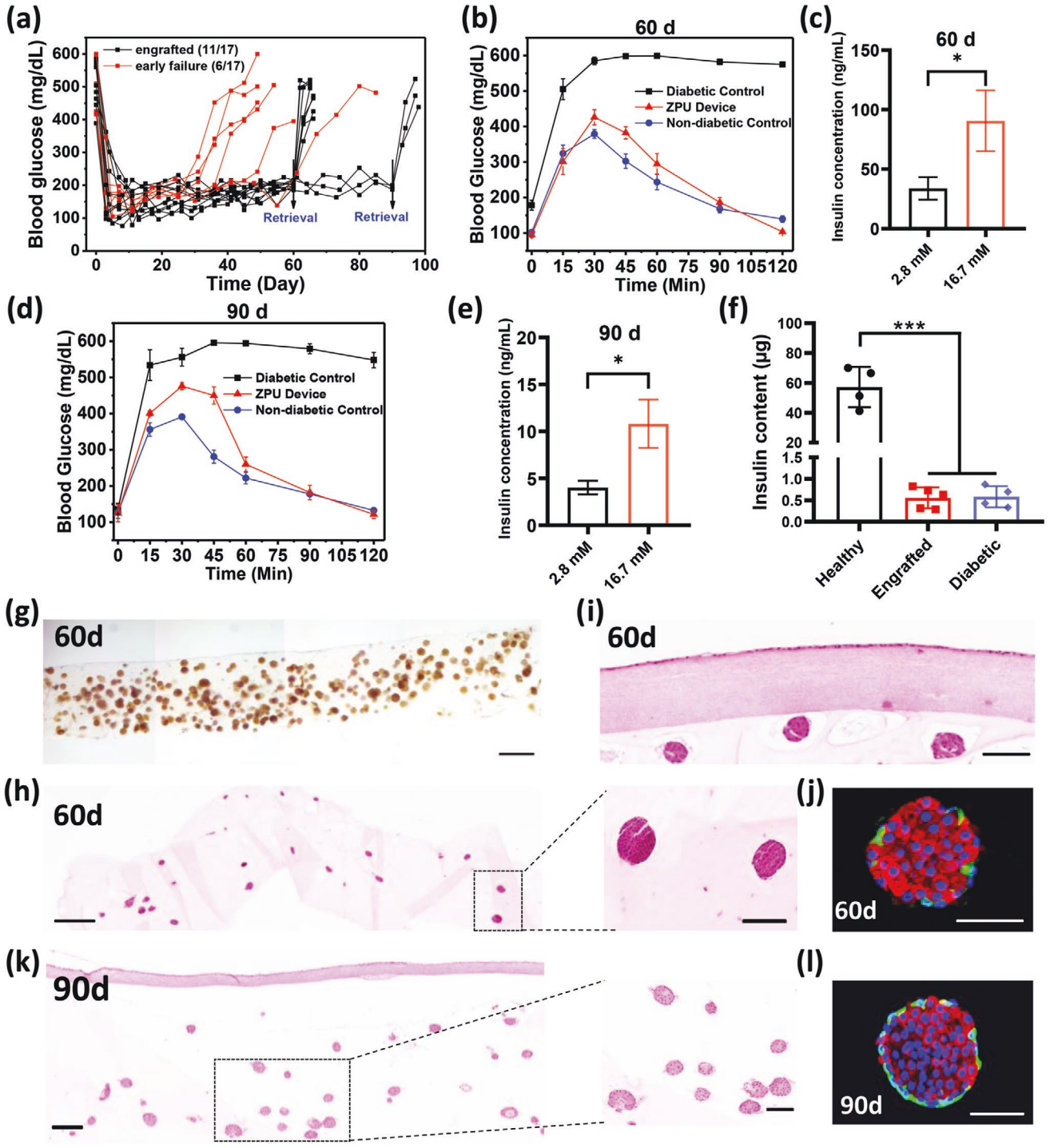

Figure 5. Demonstration of the therapeutic potential of the ZPU device in diabetic mice using rat islets. a) Blood glucose concentrations of non-fasting mice ($n = 17$). b) Intraperitoneal glucose tolerance test (IPGTT) before retrieval on day 60 ($n = 4$). c) Ex vivo GSIS of retrieved islets from the ZPU devices on day 60. Mean ± S.E.M. ($n = 3$); $^*p < 0.05$. d) IPGTT before retrieval ($n = 3$ per group) on day 90. e) Ex vivo GSIS of retrieved islets from the ZPU devices on day 90. Mean ± S.E.M. ($n = 3$); $^*p < 0.05$. f) Measurement of total insulin content of the pancreas in different groups on day 60. Mean ± S.E.M. ($n = 4$–5); $^{***}p < 0.001$. g) Bright-field image of encapsulated rat islets after retrieval on day 60 (The nanofiber membrane was removed for imaging; scale bar: 500 μm). h) H&E stained cross-sectional image of retrieved islets on day 60. Scale bar: 500 μm. i) H&E stained cross-sectional image of retrieved islet-containing ZPU device on day 60. Scale bar: 100 μm. j) Immunohistochemical staining of islets in a retrieved ZPU device on day 60. Insulin is stained red, glucagon is stained green, and nuclei are stained blue (scale bar: 50 μm). k) H&E stained cross-sectional image of retrieved islet-containing ZPU device on day 90. Scale bar: 200 μm. l) Immunohistochemical staining of islets in a retrieved ZPU device on day 90. Insulin is stained red, glucagon is stained green, and nuclei are stained blue (scale bar: 50 μm).

(Figure 5j). Finally, there was no cell entrance or escape from the device (Figure 5i and Figure S10, Supporting Information). For the 3-month transplantation experiment, histological analysis and positive insulin staining (Figure 5k,l) confirmed longer-term function of the device. Taken together, the data described above provides a proof of concept for the use of the ZPU device for T1D treatment.

3. Discussions

Although cell encapsulation represents a promising approach for T1D treatment, clinical use remains challenging, in part because of the lack of an appropriate device that meets many design requirements simultaneously. For example, hydrogel-based devices tend to have poor mechanical properties, while polymer-based ones have mass transfer constraints partially caused by fibrotic depositions. Here, we synthesized a family of ZPU polymers with tunable material properties and used electrospinning to fabricate encapsulation devices that had several desirable characteristics. The optimized ZPU device was mechanically robust with high wettability that promoted superior mass transfer as evidenced in insulin diffusion and in vitro GSIS tests.

Moreover, it is desirable for medical devices to have antifouling properties in the context of complex biological media (e.g., body fluid, blood, and cell lysates). Biofouling is a particularly serious problem for nanoporous device as proteins and cells can result in pore block and negative impact on mass transfer. The nanofibrous ZPU device was shown to be resistant to protein adsorption and cell attachment. In addition, a translatable encapsulation device should be both functional and safe, ensuring no cell escape, particularly when hESC-derived cells are used. The ZPU device with a nanofiber size of ≈281 nm completely excluded cell entrance and prevented cell escape, while still allowing sufficient mass transfer necessary for encapsulated cells.

Another key criterion of encapsulation device is the ability to mitigate the fibrotic response. The ZPU device induced cellular overgrowth as low as 10 μm in thickness for up to 6 months in mice, while the PU control device induced much thicker fibrotic overgrowth. The device also showed promising biocompatibility in large animals although more work is needed to completely eliminate tissue adhesion. We also found that the incorporation of SB group into the polyurethane improved the water content of ZPU device and attenuated the inflammatory activation of macrophages in vitro (Figure S11, Supporting Information). These data, consistent with our previous work,[10b] support that zwitterionic groups due to their strong water hydration, play an important role in material biocompatibility. To demonstrate the potential application of the ZPU device, rat islets were encapsulated and implanted in diabetic mice. The device restored normoglycemia for up to ≈3 months in diabetic mice. Furthermore, the ZPU device was potentially scalable although more work is needed to reach a clinical capacity, and completely retrievable despite tissue adhesion at the ends of the device. However, limitations exist for this study. For example, the scaled-up ZPU device, due to its softness and length, can kink and tissue adhesion occurs repeatedly at the device end in large animals. Ideally, more work must be performed to prevent kinking and avoid adhesion. Fibrosis is another challenge that has not been completely resolved and merits more investigation. Finally, more studies on large animal models including diabetic ones are needed to evaluate the function and performance of the device.

4. Conclusion

We have designed and synthesized a family of non-biodegradable and mechanically robust ZPU with various SB contents as part of the PU backbone. The ZPU polymer was processed by electrospinning to obtain nanoporous devices for islet encapsulation. The optimized ZPU device was mechanically robust and superhydrophilic with facile mass transfer and antifouling properties. We demonstrated the safety of the device by encapsulating proliferative cells and showing continuous containment of these cells. More importantly, the ZPU mitigated cellular overgrowth in mice as compared to the PU control. We also tested the ZPU device in minipigs and dogs and showed complete retrieval. Finally, we showed the function of the device in correcting diabetes in mice. The balance between safety and function makes the ZPU device a suitable candidate in developing cell encapsulation therapies for T1D and other hormone deficient diseases. The ZPU polymers may also find other biomedical applications such as catheters and implantable devices.

5. Experimental Section

Materials/Reagents: Poly(tetramethylene ether)glycol (number-average molecular weight 2000, PTMG, Sigma-Aldrich) was dried in vacuum oven prior to synthesis. 1,4-Diaminobutane, stannous octoate ($Sn(Oct)_2$), anhydrous dimethyl sulfoxide (DMSO), dichloromethane, diethyl ether, and 1,1,1,3,3,3-hexafluoro-2-propanol (HFIP) were obtained from Sigma-Aldrich. 1,6-Diisocyanatohexane (HDI), 1, 3-propanesultone, and *N*-butyldiethanolamine were purchased from the Alfa Aesar. Calcium chloride ($CaCl_2$) and barium chloride ($BaCl_2$) were purchased from EMD Millipore. Sterile sodium alginate (SLG100, 200–300 kDa MW) were purchased from FMC BioPolymer Co. (Philadelphia, PA, USA). FITC-labeled insulin, and FITC-labeled fibrinogen were purchased from Sigma-Aldrich. Rabbit anti-insulin antibodies (Cat. #ab63820) was purchased from Abcam, and mouse anti-glucagon antibody (Cat. # SAB4200685) were purchased from Sigma-Aldrich. Alexa Fluor 594 donkey anti-rabbit antibody (Cat. #A-21207) and Alexa Fluor 488 goat anti-mouse antibody (Cat. #A-11001) were purchased from Invitrogen.

Animals: Eight-weeks-old immune-competent male C57BL/6 were purchased from the Jackson Laboratory and Sprague–Dawley rats were purchased from the Charles River Laboratories (Wilmington, MA, USA). Göttingen Minipigs and beagle dogs were purchased from the Marshall Bioresources. All animal procedures were approved by the Cornell Institutional Animal Care and Use Committee.

Synthesis of 3-(Butylbis(2-hydroxyethyl)ammonio)propane-1-sulfonate (SB-Diol): *N*-butyldiethanolamine (8.05 g, 50 mmol), 1,3-propanesultone (6.7 g, 55 mmol), and dichloromethane (200 mL) were added to a 500 mL round-bottom flask. The mixture was stirred under nitrogen atmosphere for 24 h at 40 °C. Afterward, the solvent was removed using a rotary evaporator. The product was precipitated by diethyl ether and then washed with diethyl ether three times to get white powder. The chemical structure of the product (SB-Diol) was confirmed by proton nuclear magnetic resonance. ^{1}H NMR (D_2O, 400 MHz, ppm): δ 3.97 (t,

4H), 3.54 (m, 6H), 3.4 (t, 2H), 2.91 (t, 2H), 2.15 (m, 2H), 1.68 (m, 2H), 1.34 (m, 2H), 0.90 (t, 3H).

Synthesis of Zwitterionic Polyurethanes: The synthetic route of ZPU polymer was shown in Figure S1, Supporting Information. In this study, SB-Diol/PTMG were blended at various molar ratios, respectively: 0:1, 1:1, 2:1, and 4:1 (namely PU, ZPU-1, ZPU-2, ZPU-4), and were dissolved in DMSO solvent at 80 °C under nitrogen atmosphere. HDI was then added into the flask dropwise, following two droplets of $Sn(Oct)_2$ catalyst. The mixture was stirred vigorously at 80 °C for 1 h. DMSO solvent was added if the viscosity of reaction solution was significantly increased. 1,4-Diaminobutane (as a chain extender) was added into the solution dropwise and stirred for overnight at 80 °C under nitrogen protection. The molar ratio of (SB-Diol + PTMG):HDI:1,4-diaminobutane was set as 1:2:1. Afterward, the polymer solution was precipitated in diethyl ether solvent, and then washed with diethyl ether three times. The resulting white powder was then washed with DI water three times and placed in vacuum oven at 70 °C for 24 h to remove the residual solvent.

Fabrication of Zwitterionic Polyurethane Device by Electrospinning: The ZPU polymers were dissolved in HFIP solvent with sufficient stirring at room temperature. The polymer solution was loaded in a 10 mL plastic syringe (BD Biosciences) and was fed at 1.2 mL h^{-1} by a syringe pump (Harvard Apparatus, USA). The nanofibers were spun at 15 kV with a 22 G blunt needle as the spinneret. The distance between the needle tip and the collector was set to 12 cm. The rotating aluminum rods (McMaster-Carr) with different dimensions were placed in the path of the polymer solution jet and were used to collect the electrospun fibers. The rod was rotated at a speed of 400–450 rpm. After 40 min of electrospinning, the nanofibrous tubes with rods were soaked into DI water bath overnight. The tubes were then removed from the rods carefully and were dried in vacuum oven at 40 °C for 1 day. The tubes were sterilized using UV light for 6 h, and the end of the tubes was thermally sealed by hand impulse sealer (Impulse Sealer Supply, South El Monte, CA, USA) to obtain ZPU device.

Zwitterionic Polyurethane Device Characterizations: A scanning electron microscope (LEO 1550 FESEM) was used to observe the morphology of nanofibrous ZPU device. ImageJ software was used to analyze and quantify fiber diameter. Pore size of ZPU device was measured using an advanced capillary flow porometer (PMI CFP-1100-AEHXL) with a dry-wet method. Tensile tests of ZPU devices were performed under dry condition (The samples were dry) and wet condition (The samples were immersed into water for 1 h and became completely wet) using an Instron 5965 and analyzed by the software Bluehill 3.0 SOP. The samples were stretched until failure at a rate of 10 mm min^{-1}. To verify polymer chemical structure, ZPU nanofibrous membrane were analyzed by FT-IR (Fourier transform infrared spectroscopy, Bruker Vertex V80V vacuum FT-IR system). The wavenumber ranges from 400 to 4000 cm^{-1} with 64 scans. XPS (Scienta Omicron ESCA-2SR) was used to determine element composition of ZPU membrane. The binding energy (BE) scale was corrected using C_{1s} as a reference at BE of 284.6 eV. The elemental compositions were determined based on peak areas from the C_{1s}, N_{1s}, O_{1s}, and S_{2p} peaks by CasaXPS software. The hydrophilic properties of ZPU membranes were characterized with contact-angle goniometer (ramé-hart). Water absorption of nanofibrous ZPU membranes was tested using a gravimetric method. ZPU nanofibrous membranes were dried and weighed to obtain the dry weight (m_{dry}). The membranes were immersed into 0.9% saline solution and weighed to obtain the wet weight (m_{wet}). The water adsorption was calculated as $(m_{wet} - m_{dry})/m_{dry} \times 100\%$. Q500 thermogravimetric analyzer was used to study the thermal stability of the ZPU membranes. The temperature ranged from room temperature to 700 °C with a heating rate of 10 °C min^{-1} with a continuous N_2 flow of 50 mL min^{-1}. Differential scanning calorimeter was used to study the melting temperature of ZPU polymers. The temperature ranged from −50 to 250 °C with a heating rate of 10 °C min^{-1} with a continuous N_2 flow of 50 mL min^{-1}.

Protein Adsorption Assay: Protein adsorption on nanoporous ZPU membrane was evaluated using a fluorescence method. Briefly, nanoporous ZPU membranes (10 mm × 10 mm) were placed into FITC-labeled insulin or FITC-labeled fibrinogen solution (0.1 mg mL^{-1} in PBS) at room temperature for 1 h. Afterward, the membranes were gently washed three times with PBS buffer to remove loosely adsorbed proteins. Fluorescence images of ZPU membranes were taken using a fluorescence microscope (Zeiss Axioplan 2, Berlin, Germany) with 10 × lens at a fixed exposure time. ImageJ software was used to analyze and quantify the fluorescence intensity of each sample.

Cell Attachment Assay: NIH3T3/GFP mouse fibroblasts were kept in a humidified incubator with 5% CO_2 at 37 °C prior to use. The cell culture medium consisted of Dulbecco's modified Eagle medium (DMEM), 10% fetal bovine serum (FBS), and 2% penicillin streptomycin. Sterile nanofibrous ZPU membranes (10 mm × 10 mm) were washed with sterile PBS three times and placed into individual wells of a 12-well plate. 2 mL of cell suspensions at 10^5 cells mL^{-1} were added to each well and incubated with the samples for 3 days. After incubation, the membranes were washed by PBS gently and transferred to a new 12-well plate. Fluorescence images were captured using an EVOS AMF4300 imaging system.

Bacterial Attachment Assay: *E. coli* was used as a model strain to evaluate bacterial attachment on the surface of ZPU membrane. A hundred microliter of inoculum containing 10^6 CFU of *E. coli* were seeded on the ZPU membrane for 30 min to allow attaching. Then, membranes were gently rinsed with PBS buffer before staining in live/dead Baclight bacterial viability kit followed manufacturer's instructions. The stained samples were imaged using a fluorescence microscope (Zeiss Axioplan 2, Berlin, Germany). Three images from each sample were randomly captured, and the number of accumulated bacteria on the membranes were counted from captured images.

Cytokine Secretion: Murine bone marrow derived macrophages (BMDMs) used for the assay of cytokine secretion were harvested from the femurs or tibia of 6–8-week-old C57BL/6J mice (Jackson Laboratories). Cells were treated with ACK lysis buffer (Invitrogen), centrifuged, and resuspended in culture media consisting of DMEM, 10% FBS, 1% Penstrep, and 15% macrophage colony stimulating factor for macrophage differentiation. After 1 week culture, BMDMs were dissociated using a cell scraper, and seeded on the tissue culture plates at a density of 10^5 cells per well in culture media. At 6 h culture after cell seeding, PU or ZPU membranes were added and stimulated with a combination of 25 ng mL^{-1} lipopolysaccharide and 20 ng mL^{-1} interferon gamma. The membranes were incubated for 12 h and the supernatants were collected and analyzed for TNF-α secretion by enzyme-linked immunosorbent assay (ELISA) following the manufacturer's instructions (Thermofisher).

Cell Escape Test: NIH3T3/GFP mouse fibroblasts was first suspended into fibrinogen-saline solution. Thrombin and gelatin-solution was then added and mixed into the solution to get a final concentration of 0.25 U mL^{-1} thrombin, 10 mg mL^{-1} fibrinogen, and 50 mg mL^{-1} gelation with a cell density of 10^6 cells mL^{-1}. Next, 50 µL of this cell-matrix suspension was injected into the device with one-end sealed. After 10 min, another end of the device was thermally sealed. The cell-loaded devices were cultured into cell medium, and cell escape from devices was monitored and captured using fluorescence microscopy.

Insulin Diffusion Test: FITC-labeled insulin was mixed into 2% SLG100 alginate solution at a concentration of 1 mg mL^{-1}, and this alginate solution was slowly injected into calcium chloride solution with the same concentration of FITC-labeled insulin (1 mg mL^{-1}). After 10 min crosslinking, insulin-loaded alginate fibers were prepared. Excess of calcium chloride solution on alginate fibers was dried using tissue paper. The alginate fiber was cut into several small pieces with the same weight of 50 mg. A small insulin-loaded alginate fiber was placed into each one-end sealed device, followed by thermal sealing with other end. Each device was immersed and incubated into 0.5 mL of PBS solution for predetermined time points. Afterward, 0.1 mL of the solution in triplicate was taken and transferred to a 96 well plate for fluorescence reading. The excitation/emission wavelengths were 495/519 nm. Insulin concentration in PBS solution was determined by measuring fluorescent intensity against a standard curve.

Rat Islets Isolation and Purification: Male Sprague–Dawley rats from the Charles River Laboratories were used as pancreatic islet donors. Briefly,

he rat bile duct was cannulated, and the pancreas was distended by an injection of cold 0.15% Liberase (Research Grade, Roche) in RPMI 1640 media solution (RPMI = Roswell Park Memorial Institute). The pancreas was digested in a 37 °C water bath for 30 min. Islets were purified using a discontinuous Histopaque 1077 (Sigma) gradient density and collected from interphase. These islets were further purified by a series of six gravity sedimentations. Finally, purified islets were handpicked under the microscope and washed by sterile saline solution. Islets were then cultured overnight in RPMI 1640 media with 10% heat-inactivated FBS and 1% penicillin/streptomycin for further use.

Islet Encapsulation: Prior to islet encapsulation, the sterile ZPU tubes (wall thickness: 150–200 µm; diameter: 1.0 mm; length: 2.5 cm) were fabricated. One end of the devices was thermally sealed by hand impulse sealer (Impulse Sealer Supply, South El Monte, CA, USA). The cultured islets were centrifuged at 562 RCF for 1 min and washed with 0.9% saline solution. After washing, about 250 IEQ islets were re-suspended in a 2% SLG100 alginate solution. The alginate solution containing islets was loaded into the device and placed into a crosslinking buffer containing 100×10^{-3} M $CaCl_2$ and 5×10^{-3} M $BaCl_2$ solution for 10 min. After crosslinking, the device with encapsulated islets were washed 5 times with 0.9% saline solution to remove residual crosslinking buffer. The other end of the device was thermally sealed prior to implantation.

Cell Viability Assay: The islet-containing ZPU devices as described above were cultured in cell medium for 3 days. After culture, the membranes of the devices were carefully peeled off. The viability of encapsulated islets in alginate hydrogel was stained by calcium-AM (green, live) and ethidium homodimer (red, dead) using the live/dead assay following the manufacturer's instruction (Invitrogen). The fluorescence images were captured using an EVOS AMF4300 imaging system.

Transplantation and Retrieval of Device in Mice: Immune-competent male C57BL/6 mice were used for implantation. Diabetic mice were created by injecting a STZ (130 mg kg^{-1} body weight) solution (13 mg mL^{-1} in 5×10^{-3} M sodium citrate buffer solution) interperitoneally. The mice that non-fasted blood glucose levels were more than 300 mg dL^{-1} with two consecutive measurements were considered diabetic. The mice were anesthetized using 3% isoflurane in oxygen and maintained at the same rate throughout the procedure. After abdomen fur shaving and disinfection, a 1 mm incision was made along the midline of the abdomen and the peritoneal lining was exposed using blunt dissection. The peritoneal wall was then grasped with forceps, and a 1 mm incision was made using a scalpel. Two devices with 500–600 IEQ islets in total were implanted into the peritoneal cavity through the incision. The incision was closed by surgical suture. The same procedure was followed for empty device implantation. For device retrievals, the engrafted mice were kept alive after the devices were retrieved at a predetermined time point. The BG level was monitored after retrieval in order to further confirm the function of implanted devices. The retrieved device was fixed in 10% neutrally buffered formalin for staining if there are no other characterizations such as ex vivo GSIS assay or imaging.

Implantation and Retrieval of Device in Pigs and Dogs: Both implantation and retrieval processes were performed using a laparoscopic surgical technique. Briefly, pigs or dogs were anesthetized using isoflurane and oxygen throughout the surgery. Prior to implantation, the abdomen was shaved and prepared for sterile surgery. The abdomen was insufflated with CO_2 through a central laparoscopic portal to create enough space for surgical manipulation. The device was placed in a 10 mL pipette which was inserted into the abdomen through a laparoscopic port on the left side of the abdomen. A laparoscopic probe was introduced through a right-sided port to manipulate the device within the abdomen. The device was positioned near the liver in pigs and within the omentum in dogs using a trocar. After implantation, the abdomen was deflated and the port sites were closed with suture material. The retrieval procedure of devices was conducted using a method similar to that described for implantation. The device was grasped with laparoscopic Kelly forceps.

Immune Cell Populations by Fluorescence-Activated Cell Sorting Analysis: After retrieval, the fibrotic layer deposited on devices was completely peeled off using tweezers. The fibrotic layer was cut into small pieces and then stored in 50 µL 1 mg mL^{-1} collagenase solution for 1 h. Cell mass was further smashed into single cells using the plunger of a 1 mL syringe. The cell solution was filtered through 70 µm cell strainer to remove the dissociated cells, followed by another filtration through the FACS tube filter. After centrifugation, cells were washed with PBS twice. Next, cells were stained with Zombie Yellow Fixable Viability Kit (BioLegend; 423 103) following the manufacturer's instructions. The cells were blocked with 2 µL mouse TruStain FcX PLUS (anti-mouse CD16/32) antibody (BioLegend; 156 603) on ice for 10 min. Then the cells were stained with diluted Alexa Fluor 488 anti-mouse Ly-6G/Ly-6C (Gr-1) antibody (BioLegend; 108 419), Alexa Fluor 594 anti-mouse CD4 antibody (BioLegend; 100 446), Alexa Fluor 700 anti-mouse/human CD45R/B220 antibody (BioLegend; 103 231), APC anti-mouse CD11c antibody (BioLegend; 117 309), APC/Cyanine7 anti-mouse/human CD11b antibody (BioLegend; 101 225), PerCP anti-mouse CD45 antibody (BioLegend; 103 129), Pacific Blue anti-mouse CD3 antibody (BioLegend; 100 213), PE anti-mouse F4/80 antibody (BioLegend; 123 109), and PE/Cyanine7 anti-mouse CD8a antibody (BioLegend; 100 721) on ice for 30 min. Finally, stained cells were analyzed using Attune NxT flow cytometer (Thermo Fisher). Precision count beads (BioLegend; 424 902) were used to obtain absolute counts of cells acquired on a flow cytometer.

Blood Glucose Monitoring: A small droplet of blood was collected using a lancet from the mice's tail veins and glucose concentrations were measured with a commercial glucometer (Contour Next EZ Blood Glucose Meter). Mice with non-fasting BG levels below 200 mg dL^{-1} were considered normoglycemic.

Intraperitoneal Glucose Tolerance Test Assay: IPGTT assays were conducted 2 or 3 months after transplantation. Mice with ZPU devices were fasted for approximately 16 h before an intraperitoneal injection of glucose solution (2 g kg^{-1} weight). BG levels were measured at the desired time points.

In Vitro and Ex Vivo Glucose Stimulated Insulin Secretion: Krebs Ringer Bicarbonate (KRB) buffer (98.5×10^{-3} M NaCl, 4.9×10^{-3} M KCl, 2.6×10^{-3} M $CaCl_2$, 1.2×10^{-3} M $MgSO_4 \cdot 7H_2O$, 1.2×10^{-3} M KH_2PO_4, and 25.9×10^{-3} M $NaHCO_3$ supplemented with 20×10^{-3} M HEPES and 0.1% BSA (Serological)) was prepared. For in vitro GSIS studies, islet-containing ZPU devices (about 50–60 IEQ islets per device), islet-containing alginate fibers (about 50–60 IEQ islets per fiber), and the same number of naked islets were first cultured into cell culture medium for 24 h. Encapsulated or naked islets were then incubated sequentially in 5 mL of low glucose (2.8×10^{-3} M) and high glucose (16.7×10^{-3} M) KRB buffer for 1 h each under the same condition. The supernatants were collected and stored for future analysis. For ex vivo GSIS study, retrieved islet-containing ZPU devices were placed into KRB buffer supplemented with 2.8×10^{-3} M D-glucose for 30 min and incubated in KRB buffer solution supplemented with 2.8×10^{-3} M or 16.7×10^{-3} M D-glucose for 1 h. (A 12-well plate was used for the day 60 samples and a 6-well plate was used for the day 90 samples.) The supernatants were collected and stored for future analysis. Insulin content was quantified using mouse/rat insulin ELISA kit (ALPCO) following the manufacturer's instructions. Absorbance of the solution at 450 nm was measured in the Synergy plate reader (Biotek). The stimulation index (SI) was obtained as the ratio of the insulin content after high glucose (16.7×10^{-3} M) stimulation divided by insulin content after low glucose (2.8×10^{-3} M) solution.

Insulin Content in the Pancreas: To measure the total insulin content in the pancreas of the diabetic mice, healthy mice, and engrafted mice, the homogenized tissue was placed into acid–ethanol (1.5% HCl in 70% ethanol), cut into small pieces using scissors, digested overnight at −20 °C, centrifuged and neutralized with pH 7.5 Tris buffer. The supernatants were collected and stored at −80 °C for insulin content determination as described above.

Histological Analysis and Immunostaining: The retrieved devices were fixed in 4% paraformaldehyde, embedded in paraffin and then sectioned by Cornell Histology Core Facility. The samples were sliced on a microtome at a thickness of 5 µm. Paraffin sections were then stained with hematoxylin/eosin. To conduct immunofluorescence staining, the histological slides were deparaffinized followed by sequential washing in xylene, ethanol, and water. These slides were then boiled in EDTA

solution for antigen exposure. Non-specific binding was blocked with 10% goat serum for 45 min at room temperature. These slides were decanted and incubated with primary rabbit anti-insulin antibodies (1:200) and primary mouse anti-glucagon antibodies (1:200) overnight at 4 °C. The sections were washed and incubated with the FITC-conjugated secondary antibodies, Alexa Fluor 594 donkey anti-rabbit antibody (1:400 dilution) and Alexa Fluor 488 goat anti-mouse antibody (1:400 dilution), for 30 min at room temperature. Nuclei were labeled with DAPI, and fluorescence images were captured using an EVOS AMF4300 imaging system.

Statistical Analysis: Unless otherwise stated, data are expressed as mean ± S.E.M. in the experiments. A paired Student's *t*-test was used to compare two sets of quantitative data from protein adsorption, cell attachment, bacterial attachment, immune cells deposited on the device, studies of FBR to various devices, and GSIS experiments. The level of significance was labeled as ns, *, **, and ***, denoting non-significant and *p*-value of <0.05, <0.01, and <0.001, respectively.

Supporting Information

Supporting Information is available from the Wiley Online Library or from the author.

Acknowledgements

This work made use of the Cornell Center for Materials Research Facilities supported by the National Science Foundation under Award Number DMR-1719875 and the Cornell NanoScale Facility, an NNCI member supported by NSF Grant NNCI-2025233. This project was partially supported by the Hartwell Foundation, the National Institutes of Health (NIH, 1R01DK105967–01A1), and the Novo Nordisk Company.

Note: The acknowledgements section was revised on October 1, 2021, after initial publication online.

Conflict of Interest

The authors declare no conflict of interest.

Author Contributions

Q.L. and X.W. contributed equally to this work. Q.L. and M.M. conceived and designed the project. Q.L. synthesized the materials and performed experiments to characterize, test, and optimize the devices. X.W. and A.C. performed in vivo experiments in mice and analyzed the samples. J.F. and W.L. designed and performed the in vivo dog experiments. X.W., B.W., and K.W. performed immunohistochemical and immunological experiments. Q.L. and M.M. wrote the manuscript. S.F., L.-H.W., Y.Z., and J.M.M.-M. contributed to the discussions and preparation of the manuscript. All authors reviewed the manuscript and provided input.

Data Availability Statement

Research data are not shared.

Keywords

biocompatibility, islet encapsulation, nanofibrous devices, zwitterionic polyurethane

Received: April 14, 2021
Revised: May 19, 2021
Published online: August 6, 2021

[1] a) M. A. Atkinson, G. S. Eisenbarth, A. W. Michels, *Lancet* **2014**, *383*, 69; b) A. Katsarou, S. Gudbjörnsdottir, A. Rawshani, D. Dabelea, E. Bonifacio, B. J. Anderson, L. M. Jacobsen, D. A. Schatz, Å. Lernmark, *Nat. Rev. Dis. Primers* **2017**, *3*, 17016.

[2] a) T. Desai, L. D. Shea, *Nat. Rev. Drug Discovery* **2017**, *16*, 338; b) J. Yu, J. Wang, Y. Zhang, G. Chen, W. Mao, Y. Ye, A. R. Kahkoska, J. B. Buse, R. Langer, Z. Gu, *Nat. Biomed. Eng.* **2020**, *4*, 499; c) A. L. Facklam, L. R. Volpatti, D. G. Anderson, *Adv. Mater.* **2019**, *32*, 1902005; d) J. D. Weaver, D. M. Headen, M. D. Hunckler, M. M. Coronel, C. L. Stabler, A. J. García, *Biomaterials* **2018**, *172*, 54; e) R. Mahou, D. K. Zhang, A. E. Vlahos, M. V. Sefton, *Biomaterials* **2017**, *131*, 27; f) G. Orive, R. M. Hernández, A. R. Gascón, R. Calafiore, T. M. Chang, P. De Vos, G. Hortelano, D. Hunkeler, I. Lacik, A. J. Shapiro, *Nat. Med.* **2003**, *9*, 104; g) J. Yang, Z. Cao, *J. Controlled Release* **2017**, *263*, 231; h) E. Pedraza, M. M. Coronel, C. A. Fraker, C. Ricordi, C. L. Stabler, *Proc. Natl. Acad. Sci. USA* **2012**, *109*, 4245; i) X. Wang, K. Wang, W. Zhang, M. Qiang, Y. Luo, *Biomaterials* **2017**, *138*, 80.

[3] a) F. W. Pagliuca, J. R. Millman, M. Gürtler, M. Segel, A. Van Dervort, J. H. Ryu, Q. P. Peterson, D. Greiner, D. A. Melton, *Cell* **2014**, *159*, 428; b) N. J. Hogrebe, P. Augsornworawat, K. G. Maxwell, L. Velazco-Cruz, J. R. Millman, *Nat. Biotechnol.* **2020**, *38*, 460.

[4] A. U. Ernst, L.-H. Wang, M. Ma, *J. Mater. Chem. B* **2018**, *6*, 6705.

[5] a) O. Veiseh, J. C. Doloff, M. Ma, A. J. Vegas, H. H. Tam, A. R. Bader, J. Li, E. Langan, J. Wyckoff, W. S. Loo, *Nat. Mater.* **2015**, *14*, 643; b) R. Calafiore, G. Basta, *Adv. Drug Delivery Rev.* **2014**, *67*, 84.

[6] a) D. An, A. Chiu, J. A. Flanders, W. Song, D. Shou, Y.-C. Lu, L. G. Grunnet, L. Winkel, C. Ingvorsen, N. S. Christophersen, *Proc. Natl. Acad. Sci. USA* **2018**, *115*, E263; b) B. Ludwig, A. Reichel, A. Steffen, B. Zimerman, A. V. Schally, N. L. Block, C. K. Colton, S. Ludwig, S. Kersting, E. Bonifacio, *Proc. Natl. Acad. Sci. USA* **2013**, *110*, 19054; c) S. Bose, L. R. Volpatti, D. Thiono, V. Yesilyurt, C. McGladrigan, Y. Tang, A. Facklam, A. Wang, S. Jhunjhunwala, O. Veiseh, J. Hollister-Lock, C. Bhattacharya, G. Weir, D. L. Greiner, R. Langer, D. G. Anderson, *Nat. Biomed. Eng.* **2020**, *4*, 814.

[7] J. Zhang, Y. Zhu, J. Song, T. Xu, J. Yang, Y. Du, L. Zhang, *Adv. Funct. Mater.* **2019**, *29*, 1900140.

[8] a) T. Neufeld, B. Ludwig, U. Barkai, G. C. Weir, C. K. Colton, Y. Evron, M. Balyura, K. Yavriyants, B. Zimermann, D. Azarov, *PLoS One* **2013**, *8*, e70150. b) B. Ludwig, S. Ludwig, A. Steffen, Y. Knauf, B. Zimerman, S. Heinke, S. Lehmann, U. Schubert, J. Schmid, M. Bleyer, *Proc. Natl. Acad. Sci. USA* **2017**, *114*, 11745; c) C. E. Nyitray, R. Chang, G. Faleo, K. D. Lance, D. A. Bernards, Q. Tang, T. A. Desai, *ACS Nano* **2015**, *9*, 5675.

[9] a) H.-W. Chien, W.-B. Tsai, S. Jiang, *Biomaterials* **2012**, *33*, 5706; b) T. Bai, J. Li, A. Sinclair, S. Imren, F. Merriam, F. Sun, M. B. O'Kelly, C. Nourigat, P. Jain, J. J. Delrow, *Nat. Med.* **2019**, *25*, 1566; c) S.-H. Ye, Y. Hong, H. Sakaguchi, V. Shankarraman, S. K. Luketich, A. D'Amore, W. R. Wagner, *ACS Appl. Mater. Interfaces* **2014**, *6*, 22796; d) D. Dong, J. Li, M. Cui, J. Wang, Y. Zhou, L. Luo, Y. Wei, L. Ye, H. Sun, F. Yao, *ACS Appl. Mater. Interfaces* **2016**, *8*, 4442.

[10] a) Q. Liu, A. Chiu, L. Wang, D. An, W. Li, E. Y. Chen, Y. Zhang, Y. Pardo, S. P. McDonough, L. Liu, *Biomaterials* **2020**, *230*, 119640; b) Q. Liu, A. Chiu, L.-H. Wang, D. An, M. Zhong, A. M. Smink, B. J. de Haan, P. de Vos, K. Keane, A. Vegge, E. Y. Chen, W. Song, W. F. Liu, J. Flanders, C. Rescan, L. Groth Grunnet, X. Wang, M. Ma, *Nat. Commun.* **2019**, *10*, 5262.

[11] a) R. S. Ward, K. A. White, C. A. Wolcott, A. Y. Wang, R. W. Kuhn, J. E. Taylor, J. K. John, *ASAIO J.* **1993**, *39*, M261; b) G. Zondervan, H. Hoppen, A. Pennings, W. Fritschy, G. Wolters, R. van Schilfgaard, *Biomaterials* **1992**, *13*, 136.

[12] S. Jiang, Z. Cao, *Adv. Mater.* **2010**, *22*, 920.

[13] D. W. Grainger, *Nat. Biotechnol.* **2013**, *31*, 507.

[14] J. L. Knopp, K. Bishop, T. Lerios, J. G. Chase, *J. Diabetes Sci. Technol.* **2021**, *15*, 109.
[15] L. Liu, W. Li, Q. Liu, *WIREs: Nanomed. Nanobiotechnol.* **2014**, *6*, 599.
[16] Q. Liu, A. Singh, R. Lalani, L. Liu, *Biomacromolecules* **2012**, *13*, 1086.
[17] H. Wang, D. E. Christiansen, S. Mehraeen, G. Cheng, *Chem. Sci.* **2020**, *11*, 4709.
[18] S. Fuchs, A. U. Ernst, L.-H. Wang, K. Shariati, X. Wang, Q. Liu, M. Ma, *Chem. Rev.*, https://doi.org/10.1021/acs.chemrev.0c01062.
[19] O. Veiseh, A. J. Vegas, *Adv. Drug Delivery Rev.* **2019**, *144*, 148.
[20] B. C. Ward, A. Panitch, *J. Surg. Res.* **2011**, *165*, 91.